JOURNAL OF MATERIALS SCIENCE 17 (1982) 3268–3274

The crystallization characteristics of Mg–Zn metallic glasses from $Mg_{80}Zn_{20}$ to $Mg_{60}Zn_{40}$

Z. ALTOUNIAN, TU GUO-HUA*, J. O. STROM-OLSEN
McGill University, Physics Department, Ernest Rutherford Physics Building, 3600 University Street, Montreal, Quebec H3A 2T8, Canada

Using the conventional melt-spinning technique we have been able to double the range over which Mg–Zn has hitherto been made amorphous. The crystallization characteristics of the alloys have been investigated through differential scanning calorimetry (DSC), X-ray photography and measurement of electrical resistance and magnetic susceptibility. The crystallization of amorphous Mg–Zn is initiated at lower temperatures by the precipitation of fine-grained, distorted $Mg_{51}Zn_{20}$ crystals which grow into regular $Mg_{51}Zn_{20}$ crystals at the end of the crystallization process. Mg is also precipitated for the Mg-rich alloys. The mechanism for further recrystallization at higher temperatures depends on whether the alloy is Mg-rich or Zn-rich with respect to $Mg_{51}Zn_{20}$. Both recrystallization steps are shown to be in qualitative agreement with the equilibrium phase diagram. For all compositions, upon crystallization, the electrical resistivity decreases while the valence magnetic susceptibility increases, as expected for a simple s–p system. The value of the magnetic susceptibility for the composition $Mg_{70}Zn_{30}$ is in excellent agreement with the prediction of the free electron model. The deviations from the free electron model for the other compositions may be due to the simple subtraction of the large core diamagnetism (filled d-band) of Zn.

1. Introduction

Mg–Zn is rare amongst metallic glasses prepared by quenching from the melt in that neither of its components are members of either 3-, 4- or 5-d transition series. For this reason it is an attractive system for testing theories of metallic glasses, such as the Ziman liquid metal model, since complications introduced by an unfilled d-band do not arise: one might hope that Mg–Zn would act as a free electron glass. However the usefulness of Mg–Zn as a proving ground has been restricted by the very limited range around the eutectic (Fig. 1) over which it has hitherto been made amorphous. Calka *et al.* [1] have prepared glassy alloys from $Mg_{75}Zn_{25}$ to $Mg_{68}Zn_{32}$ and Calka and Matyja [2] have extended this range at the Zn-rich end to $Mg_{65}Zn_{35}$, still a rather small range for any effective systematic study. We therefore set out to see whether conventional melt-spinning techniques could be used to extend the range of glassy formation and have in fact been able to double it from $Mg_{80}Zn_{20}$ to $Mg_{60}Zn_{40}$. As a first step towards characterizing Mg–Zn alloy glasses we present the results of crystallization studies carried out by differential scanning calorimetry (DSC), X-ray diffraction and measurement of electrical resistance and magnetic susceptibility. Such studies provide not only valuable information on the glassy phase, but also provide a check on the validity of the current crystalline phase diagram.

2. Experimental procedure

Appropriate amounts of Zn (5N purity) and Mg (4N purity) to produce about 1 g samples of compositions from $Mg_{80}Zn_{20}$ to $Mg_{60}Zn_{40}$ were

*Permanent address: Lanzhou University, China.

 0022–2461/82/113268–07$03.34/0

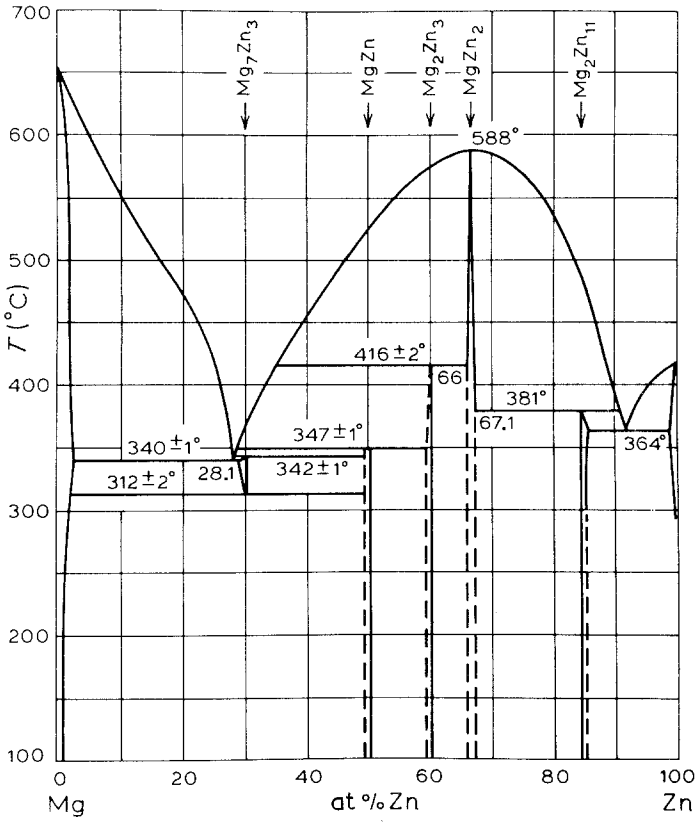

Figure 1 The equilibrium phase diagram of Mg–Zn (after Elliott [15]). Mg_7Zn_3 is more precisely designated as $Mg_{51}Zn_{20}$ in the present text.

put in a cylindrical graphite holder and sealed in a pyrex tube under 1/6 atm He. The assembly was placed into a vertical oven at 450° C for 2 h with periodical stirring to obtain homogeneous alloys. The ingot was then crushed into appropriate sizes for melt-spinning. The melt-spinning was carried out under helium at a pressure of 50 kPa. The tangential speed of the wheel was 55 m sec^{-1}. The resulting ribbons (20 to 25 μm thick) were immediately stored in liquid nitrogen, a very necessary precaution because of the low crystallization temperature of this system. Debye–Scherrer X-ray photographs, using Ni-filtered Cu$K\alpha$ radiation, showed no sharp lines after 24 h exposure. The resistance changes associated with crystallization were measured using a highly sensitive a.c. difference method [3] under a 15 kPa atmosphere of helium. The magnetic susceptibilities, χ, were measured at room temperature using the Faraday method on a Cahn electro-balance. Because of the small magnetic susceptibilities of the Mg–Zn system and the extreme brittleness of the crystallized samples, all the crystallization studies were done *in situ*. The crystallization temperatures, T_c, heats of crystallization, ΔH_c, and activation energies, E_a, were measured from thermal analysis by means of a calibrated differential scanning calorimeter, Perkin-Elmer DSC-2C, using an atmosphere of purified argon and variable heating rates from 5 to 80 K min^{-1}. X-ray diffraction studies were done before and after each exothermic peak to characterize the different stages of crystallization.

3. Results and discussion

3.1. DSC and X-ray studies

DSC measurements were carried out on all samples at increasing temperatures through the initial crystallizations and various subsequent recrystallizations until the melting point was reached. The Mg–Zn phase diagram is quite complicated, as is shown in Fig. 1, so the DSC traces are correspondingly complex. Examples of two traces are shown in Fig. 2. The temperature of the various crystallization processes for a 10 K min^{-1} heating rate are shown as a function of composition in Fig. 3, the temperature being given by the peak in the various exotherms (or endotherms in the case of melting).

The initial crystallization is *always* a doublet. X-ray studies after the first peak show lines, faint but sharp, corresponding to the structure of the phase which has been generally given as Mg_7Zn_3

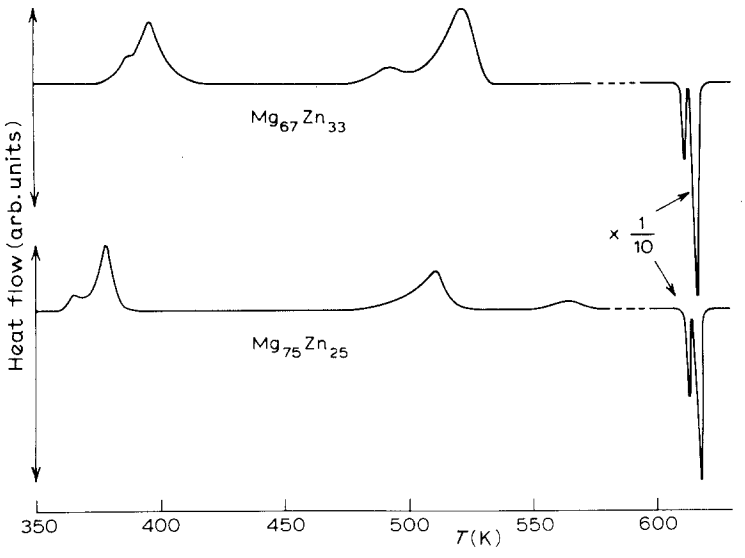

Figure 2 Complete thermograms obtained with a Perkin-Elmer DSC-2C at a heating rate of 10 K min^{-1} for $Mg_{67}Zn_{33}$ (upper trace) and $Mg_{75}Zn_{25}$ (lower trace).

but which is in fact $Mg_{51}Zn_{20}$ [4]. Co-existing with these faint lines is a diffuse amorphous ring. After the second exotherm the amorphous ring disappears and the $Mg_{51}Zn_{20}$ lines become correspondingly stronger. Alloys on the Mg-rich side of the eutectic (71.9 at% Mg) show some precipitated Mg. All of these results are consistent with transmission electron microscope studies [1, 5] on $Mg_{70}Zn_{30}$ and $Mg_{74}Zn_{26}$, which show that the first exotherm corresponds to the precipitation of the fine-grained, distorted "Mg_7Zn_3" and the second exotherm to recrystallization and growth of this phase together with crystallization of the remaining amorphous regions and (for $Mg_{74}Zn_{26}$) Mg precipitation.

At higher temperatures two more exotherms are usually seen, corresponding to further changes of structure, one of which is large and the other small. One of the most interesting features of the entire crystallization is that on the Mg-rich side of the eutectic the large peak occurs first and on the Zn-rich side the small peak occurs first. X-ray photographs show that for the three compositions $Mg_{80}Zn_{20}$, $Mg_{77.5}Zn_{22.5}$ and $Mg_{75}Zn_{25}$ the large enthalpy change associated with the first peak corresponds to the formation of metastable MgZn [6] plus further Mg precipitation and that the smaller enthalpy change associated with the second peak results from the formation of the stable MgZn phase [6]. On the Zn-rich side, where the first peak is now smaller, $Mg_{67}Zn_{33}$, $Mg_{65}Zn_{35}$, $Mg_{62.5}Zn_{37.5}$ and $Mg_{60}Zn_{40}$ show first a decomposition of Mg-deficient $Mg_{51}Zn_{20}$ into $Mg_{51}Zn_{20}$ plus Mg_2Zn_3 and then into Mg plus the stable form of MgZn, as before. Joining up the points in Fig. 3 for the small and large exotherms produces a crossover at the composition $Mg_{71.8}Zn_{28.2}$, which is identical to $Mg_{51}Zn_{20}$. Samples at this composition may be expected to show no further recrystallization before melting and such behaviour is actually observed for $Mg_{72.5}Zn_{27.5}$ for heating rates in excess of 10 K min^{-1}. In fact both this sample and $Mg_{70}Zn_{30}$ show strong dependence on heating rate, reflecting their close proximity to the peritectic composition (Fig. 1). At a heating rate of 10 K min^{-1} both show the double recrystallizations outlined above but, at heating rates greater than 20 K min^{-1}, $Mg_{72.5}Zn_{27.5}$ shows nothing and $Mg_{70}Zn_{30}$ shows only the lower temperature exotherm which itself disappears above 80 K min^{-1} heating rate. Furthermore the first endotherm at the melt (Fig. 2) almost disappears in both these alloys. Taken together these results not only confirm the existence of the $Mg_{51}Zn_{20}$ peritectic but also suggest that it has some range of stability – tentatively shaded in Fig. 3 – right down to about 100° C in contrast to the phase diagram in Fig. 1 which terminates the peritectic at 312° C.

The complete enthalpy change on crystallization, ΔH_c, is given by the area under the first *two* exotherms, as already explained. Fig. 4 shows how ΔH_c varies with composition, the errors being rather large owing to the relative smallness of the exotherms (contrast this with Cu–Zr alloy glasses [7] for example). Nonetheless, the data indicate

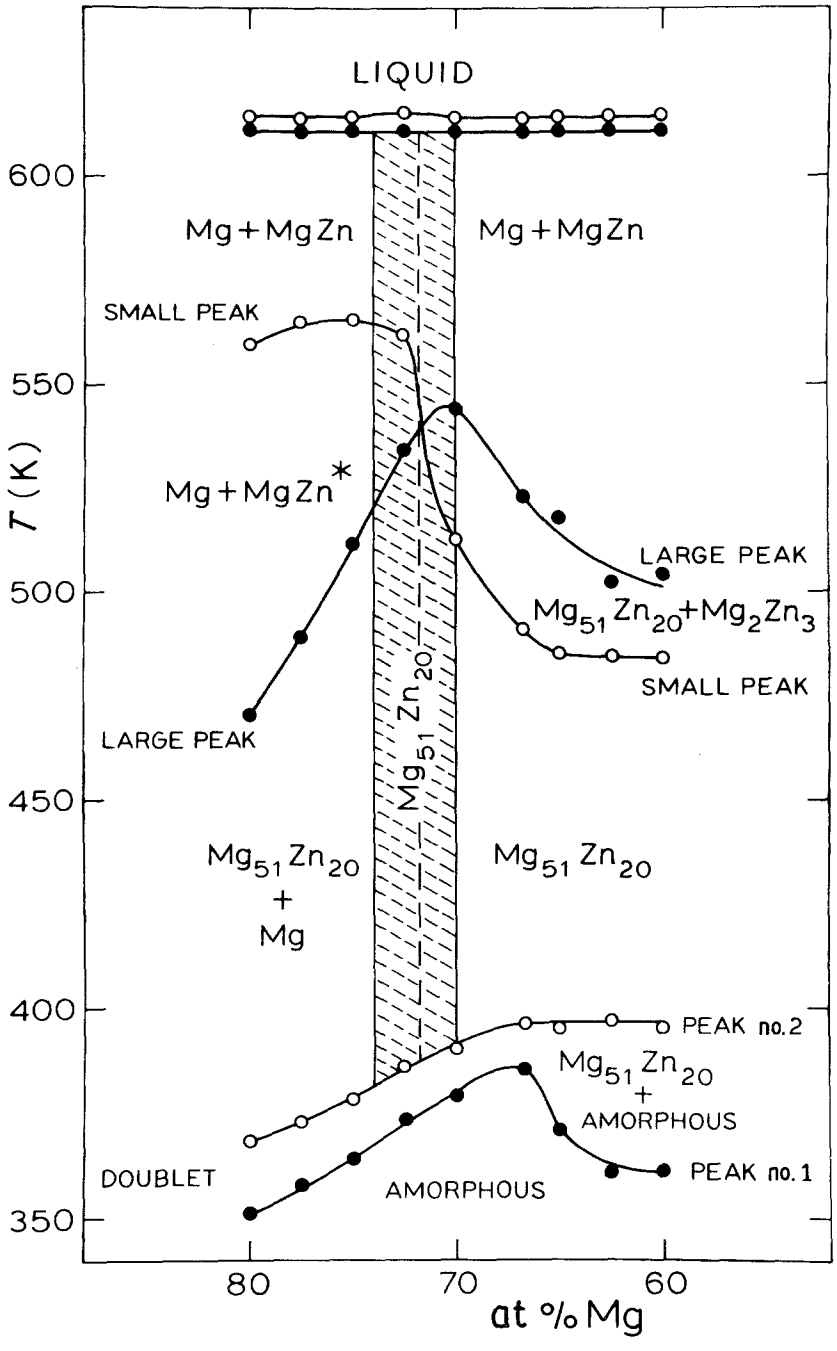

Figure 3 Crystallization, recrystallization and melting temperatures of Mg–Zn alloys corresponding to a heating rate of 10 K min^{-1} as a function of Mg content.

a probable maximum at the peritectic composition analogous to the clear maxima seen by the authors in Cu–Zr at the stable phases $CuZr_2$ and $Cu_{10}Zr_7$. As explained in that paper, a maximum is perhaps to be expected whenever a glass collapses into the relatively close-packing of a stable phase.

The activation energy, evaluated by the Kissinger method [8], is shown in Fig. 5 where we have now separated out the two crystallization peaks. The first peak which is associated with most of the crystallization is sensitive to composition showing, like ΔH_c, a maximum at $Mg_{51}Zn_{20}$. The second peak, largely associated with recrystallization, is much less sensitive to composition. Our

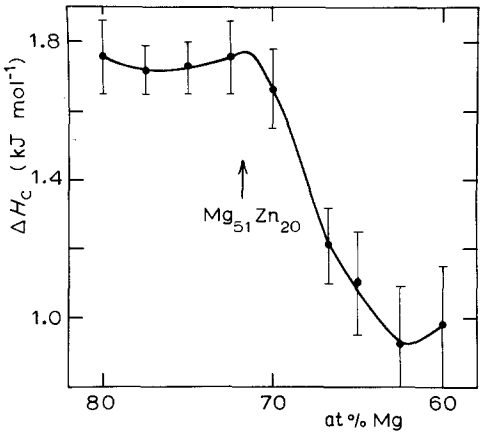

Figure 4 Enthalpy change on crystallization, ΔH_c, for Mg–Zn as a function of Mg content.

values of activation energy are in reasonable agreement with previously published data [5], where these exist, and are about a factor of two down from those for more typical transition-metal based glasses, presumably reflecting much weaker interatomic forces and perhaps also an absence of any angular dependence to the force. In Fig. 5 we have also plotted the variation of $\Delta T^* = (T_{liq}^{ideal} - T_{liq}^{mix})/T_{liq}^{mix}$ where T_{liq}^{mix} is the actual melting curve and T_{liq}^{ideal} is an "ideal" melting temperature obtained from straight line extrapolation between the melting temperatures of the pure components. ΔT^* has been suggested as a useful criterion for glass formation [9, 10], the idea being that if it is relatively large, say > 0.2, the free energy of the disordered liquid phase is sufficiently lowered to permit access to the frozen liquid, i.e. glassy, phase although it has been our experience that the above is a necessary but not sufficient condition. However, in Fig. 5 the fact that the variation of ΔT^* tracks the activation energy suggests that in Mg–Zn alloy glasses at least it can be used as a stability criterion, provided manufacturing conditions are kept constant. We have also calculated the activation energies for recrystallization into the high-temperature metastable phases. The "large" peak associated with the decomposition of $Mg_{51}Zn_{20}$ to Mg + MgZn gives a value of 1.35 + 0.15 eV (130 ± 15 kJ mol^{-1}) for all compositions. This value is in excellent agreement with the activation energy of 120 ± 3 kJ mol^{-1} for eutectoid decomposition of an equilibrated Mg_7Zn_3 phase to Mg + MgZn [11]. The activation energy for the "small" peak is difficult to determine because of its broad nature. A rough estimation gives 2.9 and 2.3 eV for the Mg-rich and Zn-rich compositions, respectively.

3.2. Electrical resistance

The change in resistance, appropriately normalized, is shown in Fig. 6. The heating rate was 10 K min^{-1}. At crystallization, the resistance typically first increases slightly then rapidly decreases; further changes follow with recrystallization and grain growth. Comparison with Fig. 2 shows that these various changes agree well with the transitions

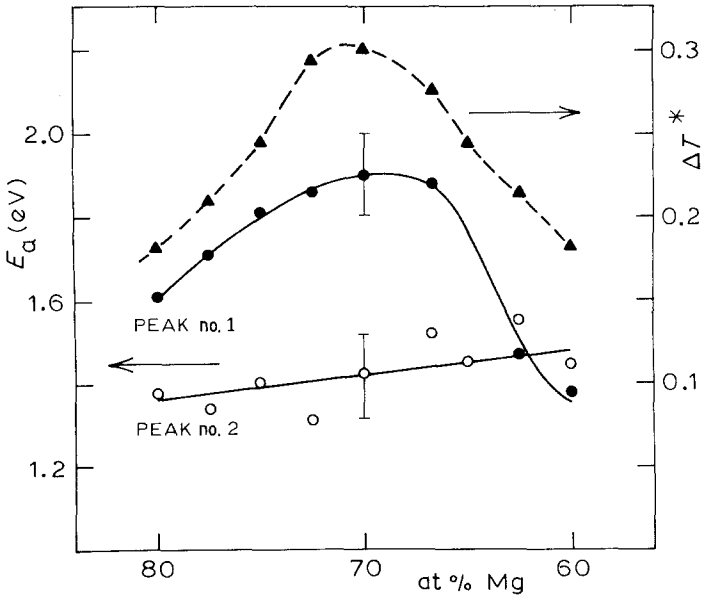

Figure 5 Activation energies for crystallization, E_a (solid line), and glass formation indicator, ΔT^* (dashed line), against Mg content in Mg–Zn.

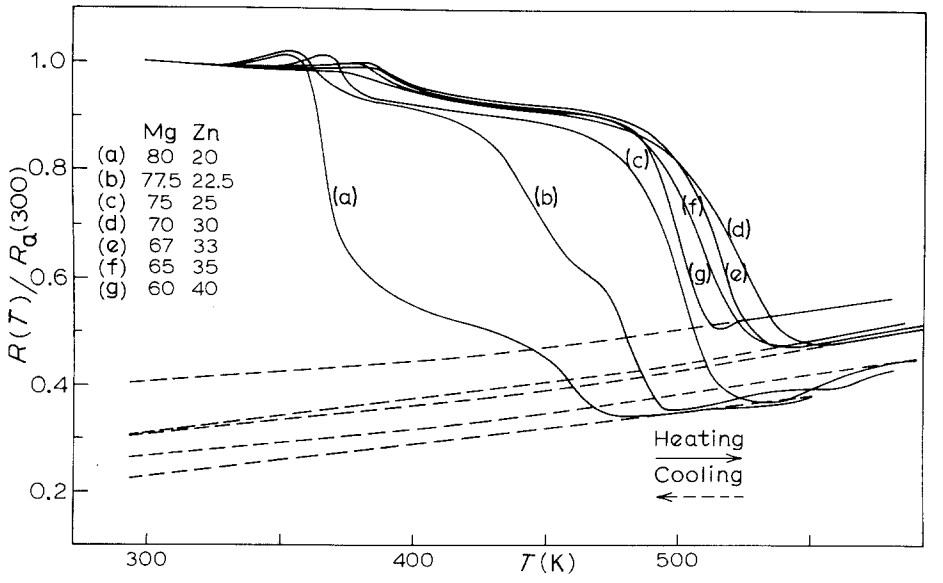

Figure 6 The change of electrical resistance with temperature, normalized to the value at 300 K.

indicated by DSC. In particular the initial increase definitely correlates with the first peak, suggesting that from the point of view of electron scattering, the precipitation of small distorted $Mg_{51}Zn_{20}$ crystals leads to a more disordered matrix than the original glassy phase. If we consider the overall fractional change in resistance from the initial amorphous phase and to the crystallized product prior to melting, we see that this increases with Mg content. Perhaps this just reflects the fact that Mg has a lower resistivity than Zn. The same result is found in the crystallized samples at room temperature.

3.3. Magnetic susceptibility

The magnetic susceptibility, χ, in all samples was independent of field up to 15 kOe, confirming the absence of any significant amount of magnetic impurity. The variation of χ in both the amorphous, χ^a, and crystalline phase, χ^c, is shown in Fig. 6. Giessen *et al.* [12] found qualitatively similar results, but a rather greater rate of change of χ with composition. Their samples, however, contained a high level of magnetic impurity so that the disagreement with our data is not surprising. The susceptibility of the crystallized samples refer to samples in the condition following the appearance of the first doublet found in DSC. Passing through the various crystalline phases gives a very complicated behaviour, as the insert in Fig. 6 shows. The valence susceptibility, χ_v, can be obtained by removing a suitably weighted average of the core susceptibility of Mg (-3.0×10^{-6} emu g^{-1} atom^{-1}) and Zn (-10×10^{-6} emu g^{-1} atom^{-1}).

A simple free electron model gives for χ_v:

$$\chi_v = \chi_{\text{Pauli}} + \chi_{\text{Landau}} = 2\mu_\beta^2(1-\tfrac{1}{3})N(E) = 0.03636\left(\frac{A}{\rho}\right)^{2/3},$$

where $N(E)$ is the density of states at the Fermi energy, A the average atomic weight and ρ the density. From our measured densities we predict a behaviour which is shown as the dashed line in Fig. 6 giving good agreement at $Mg_{70}Zn_{30}$ which is fortuitously where Mizoguchi *et al.* [13] reported good agreement with the free electron model from specific heat data. However, the differences at other compositions are not that great and could be caused by small changes in the core diamagnetism. In the case of Zn, for example, the d-band is only just filled, giving large core diamagnetism which is very sensitive to the position of the Fermi energy.

Finally, we should point out that there is *no* minimum in χ at the most stable composition (70/30) and hence no minimum in density of states here. This is in clear violation of the prediction of the model of Nagel and Tauc [14] for stability in megallic glasses.

4. Conclusions

The crystallization of amorphous Mg–Zn is initiated at low temperatures by the precipitation of fine-grained, distorted $Mg_{51}Zn_{20}$ which grow

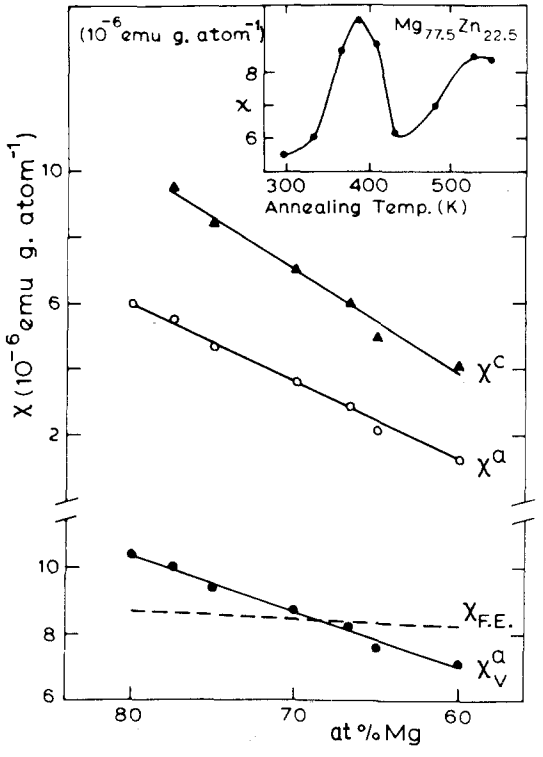

Figure 7 Plot of magnetic susceptibility of Mg–Zn alloys against Mg-content: ○, χ^a; ▲, χ^c; ●, χ_v^a; dashed line represents the free electron model prediction for χ_v^a. Insert: variation of magnetic susceptibility versus annealing temperature for $Mg_{77.5}Zn_{22.5}$. The sample was kept at each annealing temperature for 3 min.

into regular $Mg_{51}Zn_{20}$ crystals at the end of the crystallization process. Mg is also precipitated for the Mg-rich alloys. The mechanism for further recrystallizations at higher temperature depend on whether the alloy is Mg-rich or Zn-rich with respect to $Mg_{51}Zn_{20}$. Both crystallization steps are shown to be in qualitative agreement with the equilibrium phase diagram. For all compositions, upon crystallization, the electrical resistivity decreases while the valence magnetic susceptibility increases as expected for a simple s–p system. The value of the magnetic susceptibility for the composition $Mg_{70}Zn_{30}$ is in excellent agreement with the prediction of the free electron model. The deviations from the free electron model for the other compositions may be due to the simple subtraction of the large core diamagnetism (filled d-band) of Zn.

References

1. A. CALKA, M. MADHAVA, D. E. POLK, B. C. GIESSEN, H. MATYJA and J. VANDER SANDE, *Scripta Metall.* **11** (1977) 65.
2. A. CALKA and H. MATYJA, Proceedings of the Smolenice Conference on Amorphous Metallic Materials (1978), edited by P. Duhaj and P. Mrafko (VEDA Publishing House of the Slovak Academy of Sciences, Bratislava, 1980) p. 71.
3. W. B. MUIR and J. O. STROM-OLSEN, *J. Phys.* **E9** (1976) 163.
4. I. HIGASHI, N. SHIOTANI, M. UDA, T. MIZOGUCHI and H. KATOH, *J. Solid State Chem.* **36** (1981) 225.
5. P. G. BOSWELL, *Mater. Sci. Eng.* **34** (1978) 1.
6. J. B. CLARK and F. N. RHINES, *Trans. AIME* **209** (1957) 425.
7. Z. ALTOUNIAN, TU GUO-HUA and J. O. STROM-OLSEN, *J. Appl. Phys.* (1982).
8. H. E. KISSINGER, *Anal. Chem.* **29**, (1957) 1702.
9. M. MARCUS and D. TURNBULL, *Mater. Sci. Eng.* **23** (1976) 211.
10. I. W. DONALD and H. A. DAVIES, *J. Non-Crystalline Solids* **30** (1978) 77.
11. W. J. KITCHINGMAN and I. M. VESEY, *J. Inst. Met.* **98** (1970) 52.
12. B. C. GIESSEN, A. CALKA, R. RAMAN and D. J. SELLMYER, Second International Symposium on Amorphous Magnetism, Troy, New York, 1976, edited by R. A. Levy and R. Hasegawa (Plenum Press, New York, 1977) p. 197.
13. T. MIZOGUCHI, N. SHIOTANI, U. MIZUTANI, T. KUDO and S. YAMADA, *J. Physique* **41** (1980) C8-183.
14. S. R. NAGEL and J. TAUC, *Phys. Rev. Lett.* **35** (1975) 380.
15. R. P. ELLIOTT, "Constitution of Binary Alloys", 1st supplement (McGraw-Hill, New York, 1965).

Received 22 February
and accepted 23 April 1982